THE JOURNAL OF BIOLOGICAL CHEMISTRY VOL. 285, NO. 50, pp. 39249–39259, December 10, 2010

Crystal Structure of *Leishmania major* Oligopeptidase B Gives Insight into the Enzymatic Properties of a Trypanosomatid Virulence Factor*

Received for publication, June 23, 2010, and in revised form, September 20, 2010 Published, JBC Papers in Press, October 5, 2010, DOI 10.1074/jbc.M110.156679

Karen McLuskey[‡1], **Neil G. Paterson**[‡2], **Nicholas D. Bland**[§3], **Neil W. Isaacs**[‡4], **and Jeremy C. Mottram**[§4]

From [‡]*Westchem School of Chemistry and* [§]*Wellcome Trust Centre for Molecular Parasitology, Institute of Infection, Immunity and Inflammation, College of Medical, Veterinary and Life Sciences, University of Glasgow, Glasgow G12 8TA, Scotland, United Kingdom*

Oligopeptidase B (OPB) is a serine peptidase with dibasic substrate specificity. It is found in bacteria, plants, and trypanosomatid pathogens, where it has been identified as a virulence factor and potential drug target. In this study we expressed active recombinant *Leishmania major* OPB and provide the first structure of an oligopeptidase B at high resolution. The crystallographic study reveals that OPB comprises two domains, a catalytic and a propeller domain, linked together by a hinge region. The structure has been determined in complex with the oligopeptide, protease-inhibitor antipain, giving detailed information on the enzyme active site and extended substrate binding pockets. It shows that Glu-621 plays a critical role in the S1 binding pocket and, along with Phe-603, is largely responsible for the enzyme substrate specificity in P1. In the S2 binding pocket, Tyr-499 was shown to be important for substrate stability. The structure also allowed an investigation into the function of residues highlighted in other studies including Glu-623, which was predicted to be involved in the S1 binding pocket but is found forming an inter-domain hydrogen bond. Additional important salt bridges/hydrogen bonds between the two domains were observed, highlighting the significance of the domain interface in OPB. This work provides a foundation for the study of the role of OPBs as virulence factors in trypanosomatids. It could facilitate the development of specific OPB inhibitors with therapeutic potential by exploiting its unique substrate recognition properties as well as providing a model for OPBs in general.

Oligopeptidase B (OPB)[5] is a serine peptidase belonging to the prolyl oligopeptidase family (clan SC, family S9) (1). These serine-dependent peptidases all contain the active site residues Ser, Asp, and His (the catalytic triad), in this order, but can have different substrate specificities. They differ from the classical serine peptidases (trypsin and subtilisin) in that they have restricted substrate specificities and typically hydrolyze only small oligopeptides (of no more than about 30 amino acids) (2). Consequently, these enzymes can cleave biologically active peptides (such as angiotensins, Ref. 3) but not larger structured proteins.

OPB is a well-defined member of subfamily S9A (MEROPS database, Ref. 4), which also contains the archetypal S9 peptidase, prolyl oligopeptidase (POP). OPB genes have been identified in a wide range of Gram-negative bacteria, in plants, in *Leishmania* and *Trypanosoma* parasitic protozoa but not in archaea (5). Studies on OPB in trypanosomes have shown that the enzyme is an important virulence factor (6, 7). In the South American trypanosome, *Trypanosoma cruzi,* the proteolytic activity of OPB is required for calcium-signaling, which regulates trypanosome invasion of the host cell. OPB achieves this by generating an active signaling ligand that interacts at the host cell surface, mobilizing intracellular calcium and promoting the trypanosome invasion (8–10). Targeted deletion of the *OPB* gene in *T. cruzi* trypomastigotes significantly decreased the parasite virulence to mammalian host cells giving reduced parasitaemia in mice (10). In addition, the African trypanosome *Trypanosoma brucei* releases OPB into the bloodstream of infected animals upon parasite death (11–13), where it persists and remains catalytically active (14). It is thought to degrade the regulatory peptide hormone, atrial natriuretic factor, reducing its levels (11, 15) and consequently affect the control of blood volume, leading to the circulatory system lesions observed in trypanosome infections (7). In these trypanosomes, OPB has been identified as a target of several drugs (pentamidine, diminazene, and suramin) (16) and irreversible inhibitors of the enzyme exhibit anti-trypanosomal activity *in vitro* and *in vivo* (14). Consequently, OPB is regarded as a potential target for the development of therapeutic drugs and an in-depth structural characterization of the enzyme is important in understanding its substrate specificity and as an aid to any prospective drug development process.

In this study we expressed active recombinant *L. major* OPB and obtained the first structure of an oligopeptidase B at high resolution. This structure, determined in complex with the oligopeptide protease inhibitor antipain (AIP), offers a

* This work was funded by the MRC (Grant Numbers G9722968 and G0000508) and by a Wellcome Trust Value in People Award (to K. McL.).
The atomic coordinates and structure factors (code 2XE4) have been deposited in the Protein Data Bank in Europe, EMBL-EBI, Wellcome Trust Genome Campus, Cambridge, UK (http://www.ebi.ac.uk/pdbe).
⌘ *Author's Choice*—Final version full access.
[1] To whom correspondence should be addressed: Glasgow Biomedical Research Centre, 120 University Place, Glasgow G12 8TA, UK. Fax: 0141-330-4888; E-mail: Karen.McLuskey@glasgow.ac.uk.
[2] Present address: School of Biological Sciences, 3A Symonds St., Auckland, 1010, NZ.
[3] Present address: Marine Biology Laboratory, 7 MBL St., Woods Hole, MA 02543.
[4] Both authors contributed equally to this work.
[5] The abbreviations used are: OPB, oligopeptidase B; POP, prolyl oligopeptidase; PEP, prolyl endopeptidase; AIP, antipain; AMC, 7-amino-4-methoxy coumarin; Boc, *t*-butyloxycarbonyl; Z, benzyloxycarbonyl; Bz, benzoyl.

structural explanation for enzyme preference for basic substrates and gives insight into its extended substrate recognition properties. Important salt bridges between the two domains are revealed and structural features important to OPBs are identified. The structure also allows us to compare the enzyme directly to prolyl oligopeptidases, to investigate the function of residues highlighted in other studies, and provides a foundation for the study of the role of OPBs as virulence factors in trypanosomatids.

EXPERIMENTAL PROCEDURES

Expression and Purification of Recombinant Leishmania major OPB—Recombinant OPB (OPB; *LmjF09.0770*) was obtained by PCR from *L. major* genomic DNA with primers NT274 (5′-CT CAT ATG TCG TCG GAC AGC TCC GTC GCG GCC TCT GC-3′) and NT275 (5′-CC CTC GAG TTA CCT GCG AAC CAG CAG GCG CAC GGT GCT C-3′). The full-length product was ligated into pGEM-T Easy (Promega) and subcloned into pET28a(+) (Novagen) using the NdeI and XhoI restriction sites, to give pBP218. This recombinant protein has an N-terminal His_6 tag and a single amino acid difference (F25L) from the published genome sequence (17).

Overnight cultures of *Escherichia coli* BL21 DE3 (pLysS) containing pBP218 were diluted 100-fold in fresh LB medium containing 37 μg ml^{-1} chloramphenicol and 20 μg ml^{-1} kanamycin, and grown until an A_{600} of 0.6 was reached. At this density isopropyl-β-D-thiogalactopyranoside was added, to a final concentration of 1 mM and incubated overnight at 15 °C. The cells were lysed by sonication in 50 mM sodium phosphate (NaPi) pH 8.0, 300 mM NaCl. The soluble fraction was collected by centrifugation at 10,000 × *g* and filtered. The sample was applied to a metal-chelating column, charged with Ni^{2+} (Porus, Applied BioSystems). The resin was washed with 50 mM NaPi pH 8.0, 300 mM NaCl, 50 mM imidazole and the recombinant protein was eluted in the same buffer supplemented with 500 mM imidazole. Eluted samples were buffer-exchanged using a PD-10 column (GE Healthcare) and further purified by anion-exchange chromatography using a Porus HQ strong anion-exchange column (Applied Biosystems) in 50 mM Tris-HCl pH 7.0, 5 mM EDTA, using a 0–1 M NaCl gradient, and the fractions containing the purified protein were pooled. The purity of the samples were analyzed by sodium dodecyl sulfate-polyacrylamide gel electrophoresis (12% gel), followed by Coomassie staining.

Kinetic Analysis of OPB—The affinity of OPB for peptide substrates was determined by monitoring the release of the fluorescent group, AMC (7-amino-4-methoxy coumarin) from AMC-based substrates containing different amino acid components (see Fig. 1). This was achieved by incubating 5 ng of OPB with varying concentrations (0–40 μM) of benzoyl (Bz)-Arg-AMC, benzyloxycarbonyl (Z)-Phe-Arg-AMC, Z-Arg-Arg-AMC, *t*-butyloxycarbonyl (Boc)-Gly-Arg-Arg-AMC, Z-Gly-Gly-Arg-AMC, and Z-Gly-Pro-AMC (all Bachem) and measuring the change in fluorescence (λ_{ex} = 355 nm, λ_{em} = 460 nm) at 21 °C, using an EnVision 2102 plate reader (Perkin Elmer). The K_m values of peptide substrates were calculated using FIG.P (Fig.P Software Corporation) and the rate of reaction was determined by linear regression and quantified by comparison with AMC standards (Calbiochem).

OPB inhibitors were all purchased from Sigma (≥90% purity) and characterized using the conditions described above with the substrate Z-Arg-Arg-AMC (10 μM). The inhibitors leupeptin (acetyl-Leu-Leu-Arg-al) and antipain (N-(Nα-carbonyl-Arg-Val-Arg-al)-Phe) were used in the range of 0–100 μM. All IC_{50} values were calculated using FIG.P, and the K_i values determined using the Cheng-Prusoff method (18) (Fig. 1*b*). The rates of inactivation of OPB by irreversible inhibitors were determined over the course of 180 min.

Crystallization and Data Collection—Prior to crystallization, OPB was dialyzed overnight against 50 mM Tris-HCl pH 8.0, concentrated to 9.3 mg ml^{-1} and incubated with 10 mM antipain (Sigma) for 30 min (OPB-AIP). Vapor-diffusion screens were set up in 96-well MRC sitting-drop plates (Wilden) using 0.5-μl protein plus 0.5-μl reservoir against a 50-μl reservoir solution, at 20 °C. Diffraction quality crystals of OPB-AIP appeared in 2–3 days with a reservoir solution of 25% 1,2-propanediol, 10% glycerol, 5% polyethylene glycol 300 (w/v), and 0.1 M phosphate-citrate pH 4.2 (Cryo screen (Emerald Biosystems)) and reached a maximum size of 300 × 300 × 150 μM in around 2 weeks. As the crystallization solution is suitable for cryoprotection, a single crystal of OPB-AIP was taken directly from the drop and flash-cooled by plunging into liquid nitrogen before being transferred to a cryostream (Oxford Cryosystems) for data collection.

Data to 1.65 Å resolution (Table 1) were collected in-house on a MarResearch 345 image plate detector coupled to a Rigaku MicroMax 007 rotating anode generator. The crystals belong to the space group *I*222, with cell dimensions a = 95.48 Å, b = 142.78 Å, c = 208.92 Å. The unit cell contained one molecule in the asymmetric unit and a calculated Matthews coefficient of 4.2 (19) indicated a solvent content of 71%. A mercury derivative of OPB-AIP (OPB-Hg) was prepared by soaking the crystals in 1 μl of 1 mM *p*-chloromercuribenzoic acid for 30 min on ice before flash-cooling, as described previously. Data for the derivative were collected to 2.0 Å resolution on station BM14 at the European Synchrotron Radiation Facility using a MarResearch Marmosaic detector. An EXAFS scan confirmed the presence of mercury in the crystal. Problems with the x-ray source during data collection resulted in reduced data completeness (73%) but this was adequate for structural elucidation. Data were processed with D*TREK (20), HKL2000 (21), and the CCP4 program suite (22), and the final data processing statistics are shown in Table 1.

Structure Solution and Refinement—Initial phases were derived by the single-wavelength anomalous dispersion approach using the AUTOSHARP (23, 24) interface and SHELXC/D (25) to locate seven Hg^{2+} sites, with an anomalous phasing power of 0.348. Subsequent solvent density modification using SOLOMON (26) gave a good quality electron density map and an initial model, comprising 666 out of a possible 731 residues, was built using ARP/WARP (27). Interactive model building using COOT (28) extended this to 710 contiguous residues. This model was used as the template for the molecular replacement phasing of the OPB-AIP data with

TABLE 1

Crystallographic statistics

Statistics are provided for the mercury derivative (OPB-Hg) used to obtain phases and an initial model and OPB in complex with the inhibitor antipain (OPB-AIP), which was refined and used for structural analyses. Statistics for $R_{p.i.m}$ *and* R_{meas} for the OPB-AIP dataset were obtained using SCALA (22). Numbers in parentheses correspond to the statistics for the highest resolution bin.

Data set	OPB-AIP	OPB-Hg
Wavelength (Å)	1.541	1.005
Space group	*I*222	*I*222
Unit cell dimensions (Å)	a = 95.48, b = 142.78, c = 208.92	a = 96.23, b = 144.81, c = 209.95
Resolution range (Å)	32.0–1.65 (1.71–1.65)	29.80–2.00 (2.07–2.00)
No. of measured reflections	546305	292398
No. of unique reflections	167772	140002
Multiplicity	3.3 (3.0)	2.1 (2.0)
Completeness	98.4 (100.0)	73.1 (74.6)
$<I/\sigma(I)>$	8.8 (1.7)	9.7 (3.5)
R_{merge} (%)	5.7 (45.6)	5.5 (21.4)
$R_{p.i.m}$ (%)/R_{meas} (%)	3.6 (29.2)/6.8 (54.2)	
Wilson B (Å^2)	29.5	31.8
Protein residues	721	710
Hg^{2+} ions (number)	na[a]	7
Na^+/Cl^- ions	2/4	
Water/PGO/GOL/PO4 molecules	721/59/10/3	
R_{work}/R_{free}	14.0/17.8	
Root mean square for bond lengths (Å)/bond angles (°)	0.035/2.35	
Ramachandran analysis		
Favored regions	98.2	
Allowed regions	1.7	
Outliers	0.1	

[a] na, nonapplicable.

TABLE 2

Serine peptidase activity of recombinant *L. major*

The substrates consisted of the protecting groups Bz, Z, and Boc and the fluorescent group AMC. NC means that no cleavage was observed, and S.E. is the standard error of the mean.

Substrate	K_m (±S.E.)	k_{cat} (±S.E.)	k_{cat}/K_m
	μM	s^{-1}	$\mu M^{-1} s^{-1}$
Bz-Arg-AMC	4.40 ± 0.55	0.016 ± 0.004	3.6×10^{-3}
Z-Phe-Arg-AMC	3.07 ± 0.20	0.011 ± 0.001	3.6×10^{-3}
Z-Arg-Arg-AMC	0.93 ± 0.16	0.010 ± 0.002	1.1×10^{-2}
Boc-Gly-Arg-Arg-AMC	1.25 ± 0.22	0.013 ± 0.003	1.0×10^{-2}
Z-Gly-Gly-Arg-AMC	3.77 ± 0.67	0.020 ± 0.008	5.3×10^{-3}
Z-Gly-Pro-AMC	NC	NC	NC

PHASER (29). The structure was refined in the usual way using REFMAC (30), together with model building using COOT (28). Inspection of electron ($2mF_o - DF_c$) and difference ($mF_o - DF_c$) density maps identified the ligand along with water, sulfate, glycerol (GOL) and 1,2-propanediol (PGO) molecules. The refined model comprises residues 10–730 with the main chain torsion angles of all residues in the allowed regions of a Ramachandran plot (COOT). The MOLPROBITY (31) score for the structure was 1.62 (within the 83rd percentile for its resolution). Statistics are given in Table 1. The model and structure factors have been deposited into the Protein Data Bank (PDB) (32) with the code 2XE4.

RESULTS

L. major OPB—Recombinant OPB expressed in *E. coli* and purified by metal chelate affinity and anion-exchange chromatography, gave a yield of ~80 mg liter^{-1}. It did not cleave substrates after proline residues but was found to efficiently cleave after arginine residues showing similar substrate specificity to both OPB from *E. coli* (33) and *T. brucei* (34) (EcOPB and TbOPB, respectively) that have arginine specificity at the P1 position. Although the highest k_{cat} value was observed with Z-Gly-Gly-Arg-AMC (0.02 s^{-1}, Table 2), this had a relatively low affinity for the active site of OPB (K_m, 3.8 μM), and the greatest catalytic efficiency was observed with the substrates containing a di-arginine motif, Z-Arg-Arg-AMC and Boc-Gly-Arg-Arg-AMC (Fig. 1*a*), which had the lowest K_m values.

Inhibitors of clan PA(S), family S1 serine peptidases (phenylmethylsulfonyl fluoride; PMSF), clan CA, family C1 cysteine peptidases (L-trans-epoxysuccinyl-leucylamido(4-guanidino) butane; E64), aspartic peptidases (pepstatin A) or metallopeptidases (EDTA) did not inhibit OPB, and unlike OPBs from *T. brucei* (35), *T. congolense* (36), or *Streptomyces griseus* (37) neither dithiothreitol (DTT) nor iodoacetamide (IAA) had any effect on activity. However, the inhibitors antipain and leupeptin inhibited OPB with K_i values of 69 nM and 26 nM, respectively (Fig. 1*b*) and after 2 h of incubation with 10 μM of the water-soluble serine protease inhibitor 4-(2-aminoethyl)-benzenesulfonyl-fluoride (AEBSF), OPB activity was reduced by 90%.

Overall Structure—The nearly complete structure of OPB includes residues 10–730; the histidine tag, the first nine residues at the N terminus, and the final C-terminal residue are disordered and not visible in the electron density maps. The enzyme is composed of two separate domains, the catalytic and the propeller domains, connected by a hinge region composed of two linear polypeptide strands (residues 94–102 and 447–454). The structure exhibits a domain swap with the catalytic domain containing an N-terminal region (residues 1–93) and a C-terminal region (residues 455–731), whereas the propeller domain consists of residues 103–446 (Fig. 2).

The N-terminal region of the catalytic domain contains two short anti-parallel β-strands (β1* and β2*) connected by a long 16-residue loop (loop1). These are followed by an 11-residue loop containing a short 3_{10} helix (α0*) connected to a large L-shaped helix, composed of two α-helices joined by a short segment of 3_{10} helix (α1*). This envelops one side of the

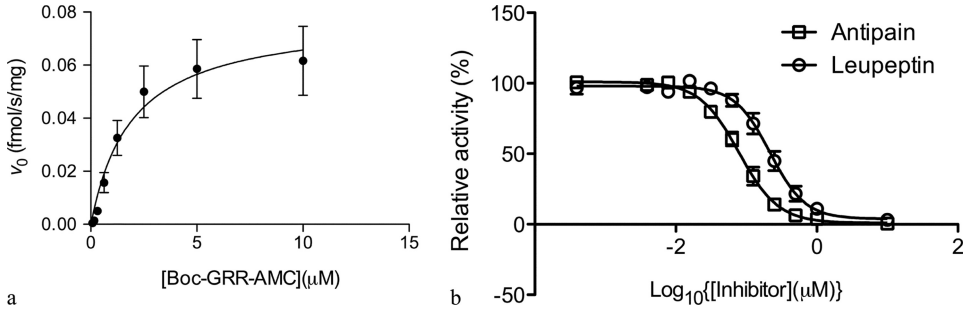

FIGURE 1. **Kinetic characterization of OPB.** OPB activity was measured by the change in fluorescence (λ_{ex} = 355 nm, λ_{em} = 460 nm) due to release of AMC from peptide substrates and quantified by comparison with AMC standards. *a*, the Michaelis-Menten kinetics of Boc-GRR-AMC (Boc-Gly-Arg-Arg-AMC) were determined by incubation of OPB (5 ng) with varying concentrations of substrate. FIG.P (Fig.P Software Corporation) was used to calculate the K_m and V_{max} values, and these data were subsequently used to determine the k_{cat} and the catalytic efficiency of the substrate. This analysis was repeated for all substrates and the results reported in Table 2. *b*, dose response curve was plotted for antipain and leupeptin and all IC_{50} values were calculated using FIG.P, and the K_i values determined using the Cheng-Prusoff equation (18): $K_i = IC_{50}/[1 + ([S]/K_m)]$, where [S] is the concentration of the substrate.

C-terminal region, which exhibits a typical α/β-hydrolase fold (38) with a central eight-stranded β-sheet, eight α-helices and seven short sections of 3_{10} helix (β1-β8, α1-α8, and α0′, α2′, α3′, α4′, α5′, α6′, α8′ (named after the helix they follow apart from α0′ which is at the start of the domain preceding β1) from the N to C terminus, respectively). Strands β1 and β2 are in an anti-parallel orientation while the remainder adopt a parallel conformation (Fig. 2*c*). The sheet is twisted and flanked by α1 and α8 on one side and α2-α7 on the other. The catalytic triad (Ser-577, His-697, Asp-662) is located on loops situated between β-strands (following β5, β7, and β8, respectively (Fig. 2, *a* and *c*)) facing the propeller domain; placing it in a large cavity at the interface between the two domains. The inhibitor, antipain is found in this cavity.

The propeller domain is a seven-bladed (B1-B7) β-propeller, with each blade composed of four β-strands (β1/1-β1/4 to β7/1-β7/4, respectively) (Fig. 2, *a* and *b*) forming an anti-parallel β-sheet. The β-strands are connected by loops that form the surface above and below the propeller and these contain one short α-helix (αA) after β1/4 (below the propeller) and two short 3_{10} helices (αB and αC) following β3/3 and β7/1 (above the propeller), respectively. The "Velcro" that has been observed to link blades B1 and B7 in other propeller proteins (*e.g.* (39, 40)) is absent and is replaced by mainly hydrophobic interactions and a single hydrogen bond between residues Gly-106 and Gln-412 (on the loops following β1/1 and αC, respectively). There is a large cavity in this domain, located near to where antipain is found, and it forms a channel filled with PGO and water molecules extending away from the inhibitor and narrowing to around 6 Å at the top of the domain. This opening is too small for the entry of an oligopeptide substrate.

Structural Comparison with pPOP—Architectural comparisons with known structures, carried out using DALILITE v.3 (41), showed that OPB is most similar structurally to the previously determined prolyl oligopeptidases (POP) (and so called prolyl endopeptidase (PEP)) structures from porcine (pPOP) (42) (PDB ID 1QFS; Z-score 46.4), *Myxoococcus xanthus* (mPEP) (PDB ID 1BKL; Z-score 46.1) and *Sphingomonas capsulata* (sPEP) (43) (PDB ID 1YR2; Z-score 44.6). POP and OPB both catalyze the hydrolysis of peptide bonds in oligopeptides but they have markedly different substrate specificities with POP cleaving peptide bonds at the C-terminal side of proline residues. Because of the similar Z-scores and the fact that pPOP and mPEP are structurally homologous, the majority of the following comparative analysis is carried out against pPOP. OPB numbering is adopted throughout, unless otherwise stated.

Using secondary structure matching (SSM, Ref. 44), the structure of OPB aligned with 620 residues of pPOP with a root mean square deviation (rmsd) on Cα-positions of 2.19 Å and a sequence identity of 22% (Fig. 3). The largest differences are in the loop regions (Fig. 3*a*). Loop A, a 19-residue loop in pPOP situated between β3/2 and β3/3 (42) (implicated in controlling substrate access to the active site (45)) is only five residues long in OPB. Conversely, Loop 1 in OPB is 16 residues long but contains only two residues in pPOP, and Loop 2 a 14-residue loop in OPB between β6/3 and β6/4 is only five residues long in pPOP. Smaller changes include the insertion of a short 3_{10} helix (αC) at the start of the loop between β7/1 and β7/2 in OPB and a shortening in OPB, by five and three residues respectively, of two longer loops found in pPOP preceding β7 and β8. Overall, SSM revealed that 82% of the secondary structural elements SSE of OPB align with those of pPOP. The overlay of the catalytic domains, with 87% SSE matching, 28% sequence identity and an rmsd of 1.4 Å, is much tighter than that of the propeller domains (74% SSE matching, 17% sequence identity and an rmsd of 2.4 Å) (Fig. 3).

Active Site and Substrate Binding—Characteristic of α/β hydrolases, Ser-577 is at the tip of a sharp turn, referred to as the nucleophilic elbow, leaving the serine OH group exposed to the catalytic His-697 on one side and the inhibitor on the other (Fig. 4*a*). A network of hydrogen bonds links His-697 to both Ser-577-OG and Asp-662-OD2 (NE1 and ND1, respectively) and Asp-662 (OD1 and OD2) to main chain amide groups from Arg-664 and Val-665, and a well-ordered water molecule, respectively.

Throughout this work, the convention of Schechter and Berger (46) is used for defining substrate residues and subsites. The oligopeptide inhibitor antipain, consists of *N*-carboxy-l-phenylalanine (FC0), Arg, Val, and arginal (Rgl); residues P4, P3, P2, and P1, respectively. It forms a covalent hemiacetal adduct with Ser-577 (Ser-577-OG to the main

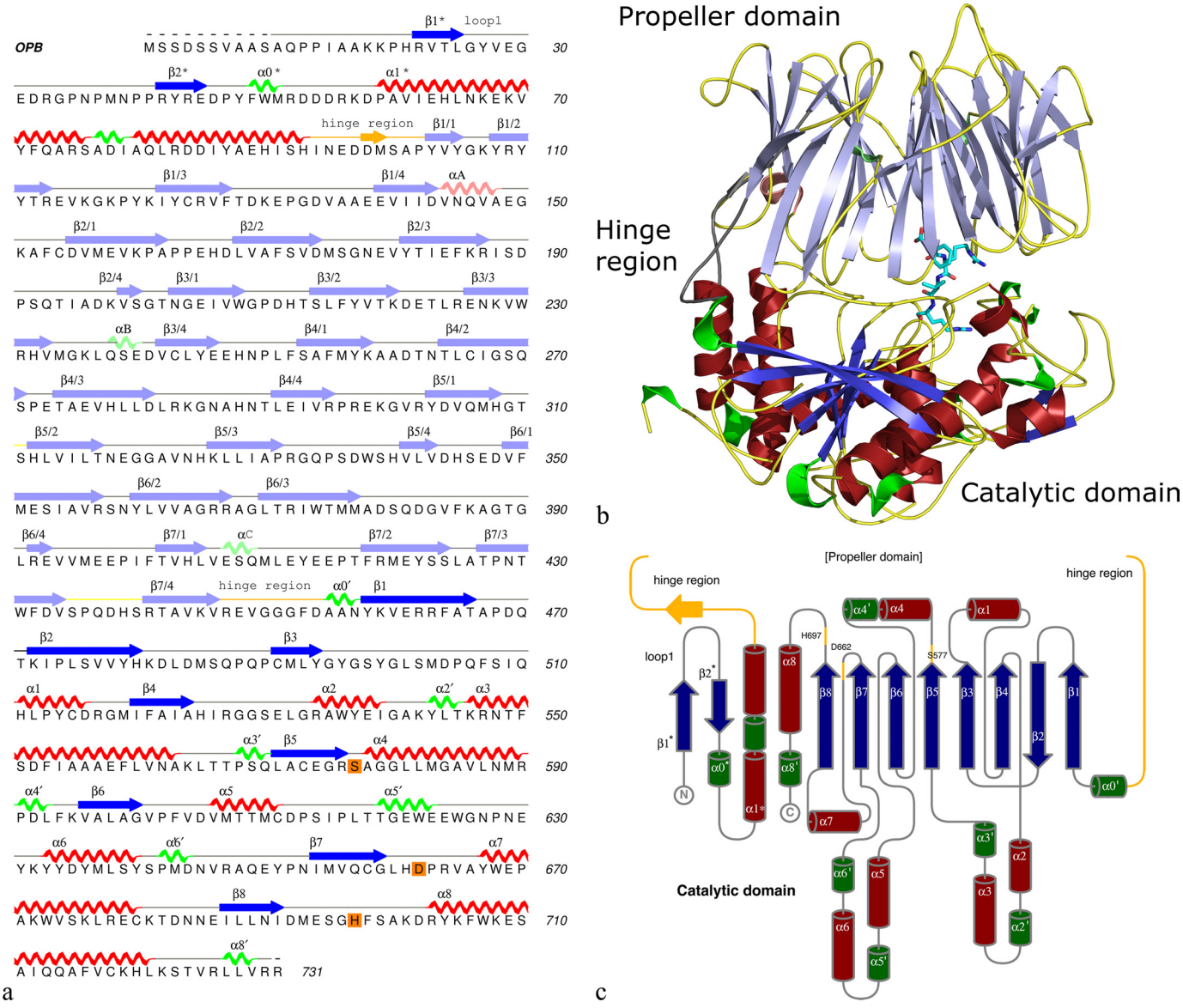

FIGURE 2. **Sequence and structure of OPB.** General loop regions are shown in *gray* (*yellow* in *b*), α-helices in *red*, β-strands in *blue*, and 3_{10} helices in *green*. The hinge regions between the two domains and the catalytic triad are highlighted in *orange* (*a* and *c*), and the catalytic domain is represented by deep colors and the propeller by pale colors. *a*, the amino acid sequence of *L. major* OPB with the assigned secondary structure (STRIDE, (53)). This figure was made using ALINE (54). *b*, the tertiary structure of OPB with antipain bound in the active site. OPB is represented as a *scheme*, and antipain is colored *cyan* and shown in *stick mode*. *c*, the topology of the OPB catalytic domain prepared with TOPDRAW (55). The propeller domain is situated at the ends of the hinges, highlighting the domain swap in the catalytic domain. All three-dimensional figures were produced using PyMOL (56).

chain C of P1) and is anchored non-covalently in the S1-S4 binding pockets of the protein, extending from the catalytic site into the propeller domain. The entire molecule of AIP can be observed in the crystal structure (Fig. 5) with P1-P3 being better defined than P4 (as seen by higher B-factors). All of the hydrogen bonding interactions between the protein and inhibitor come from the catalytic domain, apart from a single interaction between the P3 guanidino group of AIP and Ser-253-OG, which is part of the propeller domain. The guanidino group of Arg-664 (NH1) makes the sole contact to the P4 residue through its ureido carbonyl. There are no other contacts to the P3 or P4 residues, and this part of the inhibitor is found in a solvent-filled cavity.

The oxyanion binding site (P1 carbonyl oxygen) is stabilized by two hydrogen bonds. In the α/β hydrolase family these are typically from two main chain amide groups (38). In OPB, the first is from a main chain amide group (Ala-578) located adjacent to the catalytic serine. However, the second is from the OH group of a Tyr (Tyr-496) (Figs. 6*a* and 7*b*). This provides a better proton donor than a backbone NH group and an identical arrangement is found in pPOP (42).

Along with the covalent adduct and the oxyanion binding site, the P1 residue of AIP is anchored in the active site through interactions with Glu-621-OE1 and Tyr-499-OH which form hydrogen bonds to the P1 guanidino and main chain amino groups, respectively (Figs. 6*a* and 7*b*). Glu-621 and Tyr-499 are both conserved throughout the OPB family and are also hydrogen bonded together (Glu-621-OE2 to Tyr-499-OH). Glu-621 is further stabilized through interactions with highly conserved Trp-625 (NE1 to Glu-621-OE1) and a

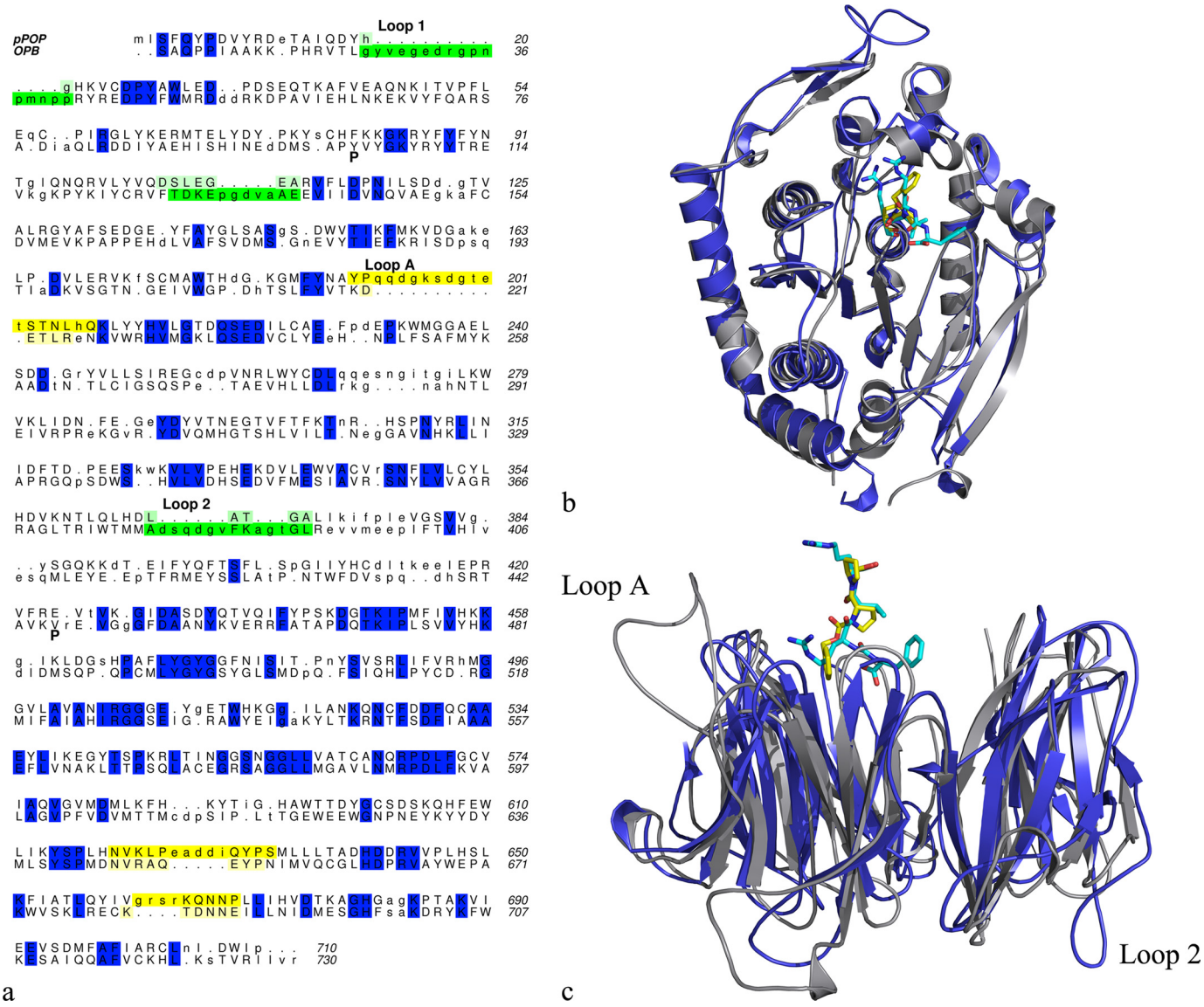

FIGURE 3. **Sequence and structural comparison of *L. major* OPB and porcine POP.** *a*, primary sequence alignment based on structure of pPOP and OPB (*SSM*, Ref. 44). Conserved residues are shown in *blue*. Additional loops in OPB are highlighted in *green* with the corresponding loop residues in POP highlighted in *pale green*. Additional loops in POP are highlighted in *bright yellow* with the corresponding loop residues in OPB in *pale yellow*. The start and end of the propeller domain in OPB is marked with a *P*. This diagram was produced using ALINE (54). *b*, structural overlay of the catalytic domains of OPB (*blue*) and pPOP (gray). The pPOP inhibitor, Z-Pro-prolinal, and OPB inhibitor, antipain, are shown in *yellow* and *cyan*, respectively and represented by *sticks*. *c*, structural overlay of the propeller domains of OPB (*blue*) and pPOP (*gray*). The corresponding inhibitors are shown, and their backbones overlay well. Structural overlays were produced using SSM (44).

well-ordered water molecule (A2687) coordinating to Glu-621-OE2 and the P3 carbonyl oxygen (not shown). Glu-621 is most likely to be responsible for the enzyme substrate specificity in P1, while Tyr-499 appears to have a role in both orientating Glu-621 and stabilizing the P1 arginine (Tyr-499 is Phe in pPOP).

The S1 binding pocket is well organized (Fig. 6*a*). The P1 guanidino group stacks against a conserved Phe (Phe-603), making a cation-π interaction, and also forms hydrogen bonds with the carbonyl oxygen of Arg-664 and two well-defined water molecules (A2580 and A2662). These solvent molecules are in turn stabilized through bridging interactions with conserved residues Thr-618 and Pro-616, and Glu-669 and Ala-666 (conserved only in the protozoa), respectively. These residues do not align with any residues in the pPOP structure and are likely to be involved in stabilizing Arg/Lys in the S1 binding pocket.

The S2 subsite of OPB is less specific for substrate side chains than the S1 pocket but, like other members of the family (47, 48), it does show a preference for cleaving after basic residues. In the structure, the S2 binding pocket contributes a single hydrogen bond from Arg-664-NH1 to the P2 carbonyl oxygen. A similar contribution from Arg-643 is found in pPOP (Fig. 7*a*) and consequently, this is unlikely to contribute to the enzyme substrate specificity. In OPB, the S2 binding pocket has a large cavity at one side and there are no acidic functional groups that could be responsible for the enzyme substrate specificity at this position.

To investigate possible interactions important for S2 substrate specificity, a tri-Arg peptide was modeled onto the anti-

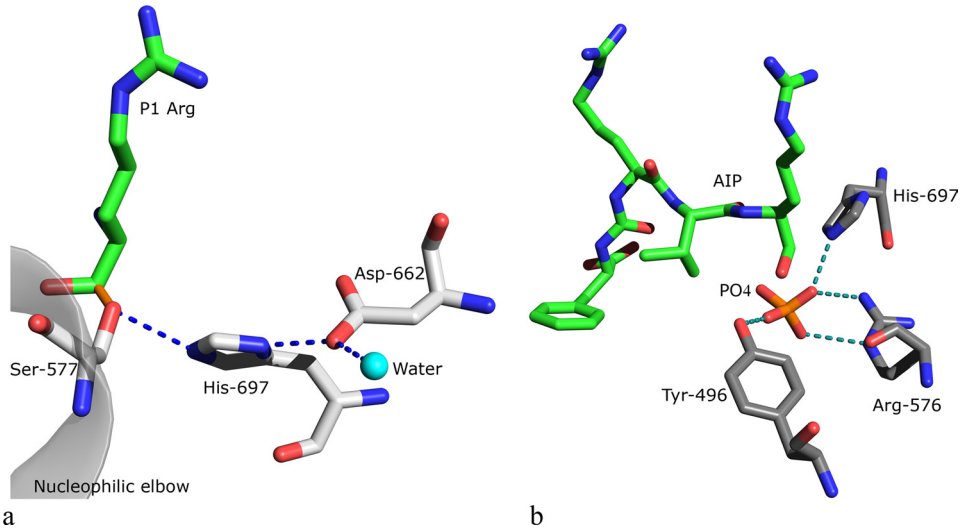

FIGURE 4. **The catalytic triad and phosphate binding site of OPB.** Amino acids are shown in stick mode colored according to atom type: (C, *silver/gray*; N, *blue*; O *red*, and P *orange*). The carbon atoms in the P1 Arg are shown in *green*, and *dashed lines* represent hydrogen bonds. *a*, covalent adduct is represented by an *orange line*, and the network of hydrogen bonds is shown as *blue dashed lines*. Water is shown as a *cyan sphere*, and the nucleophilic elbow of OPB is represented in *oval cartoon mode*. *b*, PO_4 molecule sits around 3 Å away from the hemiacetal carbon of antipain potentially mimicking the position of a P1′ residue.

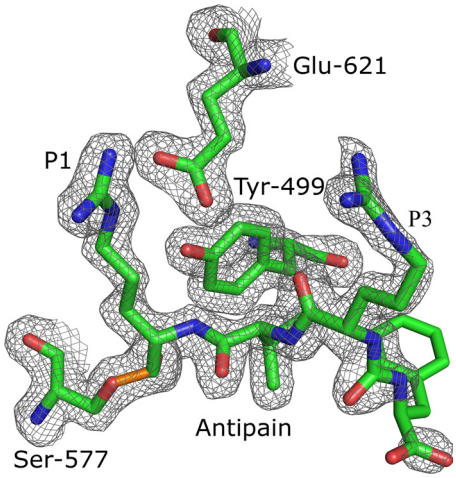

FIGURE 5. **Electron density map for antipain and selected residues in the S1 binding pocket.** The $2mF_o - DF_c$ is contoured at 1.5 σ and is shown as a *gray mesh* around Ser-577, Glu-621, Tyr-499 of OPB, and the bound antipain molecule. Amino acids are shown in *stick mode* colored according to atom type: (C, *green*, N, *blue*, and O, *red*), and the covalent adduct is represented by a *solid orange line*. The P1 and P3 residues of the antipain are labeled for clarity.

pain structure using COOT (28). The most commonly observed Arg rotamer found in protein structures (49) was used in position P2 and revealed a possible single hydrogen bond between the P2 guanidino group and the carbonyl oxygen of Tyr-499 (Fig. 6*b*). Other models, built with alternative rotamers either clashed with the backbone of the protein or existed in a large solvent-filled cavity. Tyr-499 sits on a flexible loop between β3 and α1 surrounded by several conserved Gly residues. It has a top-to-tail orientation with the modeled P2 Arg producing hydrophobic anti-parallel stacking between the two residues at around 3.6 Å. Tyr-499 appears to stabilize the substrate at P2 through this stacking and the lone hydrogen bond.

In the structure, a single phosphate moiety is located ~3 Å away from the hemiacetal carbon of AIP. This is stabilized in a binding site by hydrogen bonds from Tyr-496-OH, the catalytic His-697 (NE2) and Arg-576-NE and NH_2 (Fig. 4*b*). This appears to mimic the P1′ amino acid, which would sit at the C-terminal side of the scissile bond.

Domain Interface—An investigation of the interface between the catalytic and propeller domains was carried out using PISA (50). This showed that it comprises 123 residues and is stabilized by 29 hydrogen bonds as well as salt bridges (SB)s between five pairs of residues (Table 3), creating a buried surface area of around 2200 Å^2.

The salt bridges appear to play an important role in the stabilization of the interface. SB1 is found between Arg-664 in the catalytic domain (cat) (which was found stabilizing the bound inhibitor (above)) and Glu-179 from the propeller domain (prop). SB2 between Glu-538 (cat) (which is conserved in the OPB family) and Arg-302 (prop) is in an unusual environment with Arg-302 adopting a dual conformation. In one conformation, the inter-domain salt bridge is formed, but in the other, Arg-302 forms a hydrogen bond to the main chain O of Ser-271 in the same domain. Interestingly, Arg-534 (cat) sits in close proximity and is also found in a dual conformation. In one conformation it forms a hydrogen bond to nearby Ser-530 (cat) and in the other it forms an intra-domain salt bridge with Glu-538. Electrostatic repulsions prevent both Arg-302 and Arg-534 simultaneously interacting with Glu-538. SB3 between Asp-504 (cat) and Arg-366 (prop) makes another stable bond across the interface. In the OPB family, Arg-366 is conserved and Asp-504 is always an acidic residue (Asp or Glu). Finally, highly conserved Arg-703 (cat) reaches into the propeller domain, interacting with both Glu-96 and Glu-114 (SB4 and SB5, respectively).

DISCUSSION

Active Site Comparison with pPOP—OPB is structurally similar to pPOP (Fig. 3 and (42)), but is markedly different in its substrate specificity cleaving after basic residues as op-

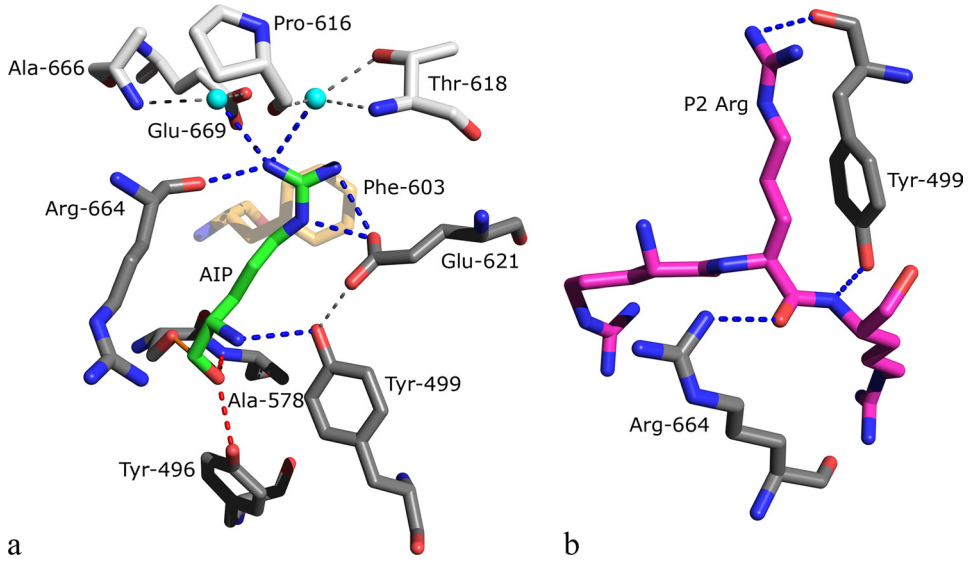

FIGURE 6. **The S1 (*a*) and S2 (*b*) binding pockets of OPB.** Amino acids are shown in *stick mode* colored according to atom type: (N, *blue* and O, *red*), the color of the carbon atoms differs depending on the residue type. *a*, residues found directly binding to the P1 residue are colored *gray*, those indirectly binding are colored *silver*, Phe-603 is colored *sand*, and the P1 Arg is colored *green*. Waters are depicted as *cyan spheres*. Hydrogen bonds in the oxyanion binding site are represented by *red dashed lines* and covalent adduct is shown as *solid orange line*. Direct hydrogen bonds to the P1 Arg are represented by *blue dashed lines*, and indirect bonds in the binding pocket are shown as *thin gray dashed lines*. For clarity, only the P1 residue of antipain is shown, and Trp-625 is omitted from the figure. Glu-621 is the only residue found to hydrogen bond to the P1 guanidino group via its side chain. *b*, modeled tri-Arg peptide in the S2 binding pocket of OPB. Residues and the inhibitor are colored with *gray* or *magenta* C atoms, respectively. *Blue dashed lines* represent hydrogen bonds. The modeled P2 Arg was found to form a stacking interaction with Try-499; no other interactions were found using alternate rotamers.

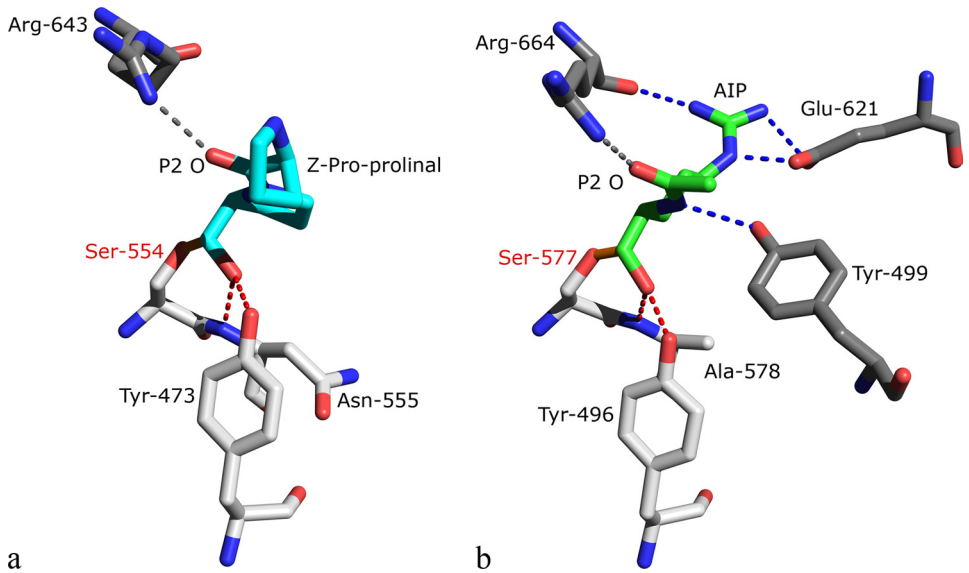

FIGURE 7. **Comparison of the interactions to the P1 residues (including the P2 O atoms) of pPOP (*a*) and OPB (*b*).** Amino acids are represented as in Fig. 2. The carbon atoms of residues involved in oxyanion binding are colored *silver*, whereas those of Z-Pro-prolinal and antipain are colored *cyan* and *green*, respectively. Only the P1 residues of the inhibitors (including the P2 carbonyl oxygen (P2 O)) are shown for clarity. The covalent adduct is shown as an *orange line*, and hydrogen bonds are represented by *dashed lines*. Those involved in oxyanion binding are shown in *red*, those to the P2 O in *gray*, and those to the P1 residue (excluding oxyanion binding) are shown in *blue*.

posed to proline. The structure of pPOP contains the inhibitor benzyloxy-carbonyl-prolyl-prolinal (Z-Pro-prolinal) bound in its active site allowing the binding pockets of the two enzymes to be compared. Calculating the electrostatic surface around the binding pockets of the two enzymes (GRASP, Ref. 51 and data not shown) reveals that there is a much less hydrophobic and more acidic environment around the inhibitor in OPB than in pPOP.

OPB functions as a serine peptidase and the three-dimensional alignment of the Cα positions of OPB on to pPOP (SSM, (44)) closely overlays the residues involved in their catalytic triads, including the well-ordered water molecule, suggesting a similar reaction mechanism for both enzymes. In addition, superimposing the two enzymes, overlays the P1-P3 backbone of the AIP molecule onto the backbone of the inhibitor in pPOP (Fig. 3*c*).

The identical hydrogen bonding to their oxyanions from a main chain amide and the hydroxyl group of a Tyr (Fig. 7) suggests that this stabilization may be specific for this family of serine peptidases. There are no other hydrogen bonds to

TABLE 3
Inter-domain salt bridges found in OPB

Salt-bridge no.	Catalytic domain	—	Propeller domain	Distance
				Å
SB1	Arg-664-NH_2	—	Glu-179-OE1	2.78
SB1	Arg-664-NH_2	—	Glu-179-OE2	3.66
SB1	Arg-664-NE	—	Glu-179-OE2	2.80
SB1	Arg-664-NE	—	Glu-179-OE1	3.37
SB2	Glu-538-OE2	—	Arg-302-NE	3.16
SB2	Glu-538-OE2	—	Arg-302-NH_2	3.95
SB3	Asp-504-OD1	—	Arg-366-NH1	2.76
SB3	Asp-504-OD2	—	Arg-366-NH_2	3.11
SB3	Asp-504-OD2	—	Arg-366-NH1	3.20
SB4	Arg-703-NH_2	—	Glu-96-OE1	3.68
SB5	Arg-703-NH_2	—	Glu-114-OE2	3.58

the P1 residue in Z-Pro-prolinal (Fig. 7*a*). In contrast, in the OPB structure the guanidino group of the P1 arginine is stabilized through hydrogen bonds from Glu-621 and Arg-664, and the P1 amide interacts with Tyr-499 (Fig. 7*b*). In addition, the P1 residue is stabilized through a cation-π interaction with Phe-603 (Fig. 6*a*), which overlays with Val-580 in pPOP.

In OPB, Arg-664 stabilizes AIP through interactions with the P2 carbonyl oxygen and forms SB1 with Glu-179. In pPOP, Arg-643 also forms a hydrogen bond to the P2 carbonyl oxygen of the bound inhibitor (Fig. 7*a*) and a salt bridge across the domain interface. Interestingly, mutations that prevent the formation of this salt bridge in mPEP resulted in a >99% loss of activity in the enzyme (43). Consequently, it appears that Glu-179 accurately positions Arg-664 in the binding pocket, which then plays an important role in stabilizing the inhibitor, and may represent a common mechanism in oligopeptidases.

S1 Subsite Specificity—Structural studies of OPB and a comparison with pPOP show that Glu-621 appears to play a pivotal role in OPB preference for basic substrates. The significance of this residue in determining the P1 substrate specificity of OPB is further supported by mutagenesis studies carried out on OPB from *Salmonella enterica* (sOPB) (48). In sOPB, the point mutations Glu-576-Ala (Glu-621 in OPB) and Glu-578-Ala (Glu-623 in OPB) resulted in significant changes in the hydrolysis of Cbz-Arg-AMC (simultaneous replacement of both residues abolished activity) and led to the speculation that both residues were involved in defining P1 specificity and directing OPB cleavage C-terminal to basic residues (48). The structure of OPB endorses this for Glu-621, however the functional group of Glu-623 sits around 14 Å away from the inhibitor forming part of an inter-domain hydrogen bond with Ser-271 (Fig. 8). This suggests that while Glu-621 is important in defining P1 specificity, the role of Glu-623 is subtler and it is likely to be important in holding the two domains in place for catalysis to occur.

S2 Subsite Specificity—Substrates with di-arginine motifs had particularly low K_m values in our assays and modeling an Arg at the P2 position of the bound AIP, resulted in a hydrophobic stacking interaction with Tyr-499 (Fig. 6*b*). In sOPB and TcOPB, Arg and Lys were found to be equally acceptable in P2, hydrolyzing with similar k_{cat}/K_m values (47, 48). Mutating the P2 position of AIP to Lys results in a similar hydrogen-bonding pattern (to the P1 amide) and hydrophobic stacking

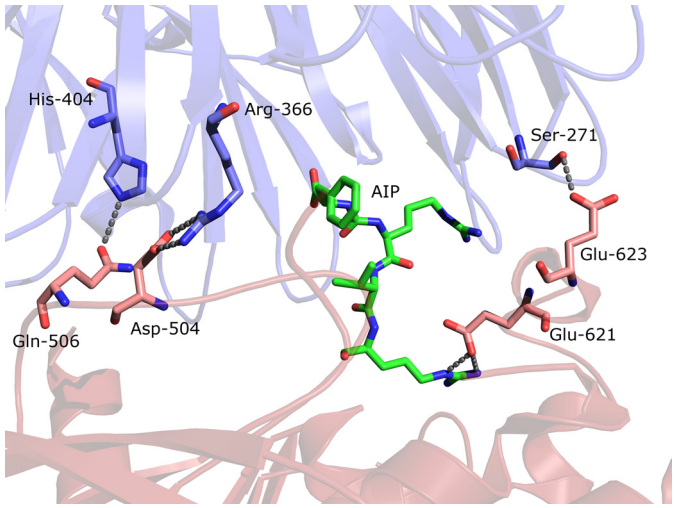

FIGURE 8. **Inter-domain interactions involving residues shown to be important in substrate specificity.** OPB is depicted as a scheme with the catalytic domain in *red* and the propeller domain in *blue*. Antipain and the highlighted residues are shown in *stick mode*, and *dashed lines* represent hydrogen-bonding interactions. Oxygen and nitrogen atoms are colored *red* and *blue*, respectively, and carbon atoms are shown in *pink*, *slate*, and *green* for residues in the propeller domain, the catalytic domain and antipain, respectively. Glu-623 was proposed to be part of the S1 binding pocket whereas Gln-506 and Asp-504 were thought to be involved in P2 binding (48).

with Tyr-499, suggesting that Tyr-499 could contribute to stabilizing both Arg and Lys at position P2.

S2 substrate specificity was also investigated in sOPB using mutagenesis (48). The double point mutations Asp-460-Thr and Asp-462-Asn (Asp-504 and Gln-506 in OPB, respectively) were found to have no effect on the hydrolysis of Cbz-Arg-AMC but dramatically reduce hydrolysis of Cbz-Arg-Arg-AMC. This effect was considerably less when a hydrophobic residue was in position P2 (in Cbz-Phe-Arg-AMC) suggesting that these residues were involved recognizing basic side chains in P2. In OPB, these residues were not found in the S2 binding pocket but were instead involved in inter-domain interactions (Fig. 8). Asp-504 forms part of SB3, a bidentate salt bridge across the two domains. It does not interact with the P2 position of the inhibitor and sits around 13 Å from the functional unit of the modeled P2 Arg. Gln-506 also forms a hydrogen bond across the domain interface to His-404 (prop), sitting at a similar distance from the modeled P2 functional unit. Consequently, in OPB these residues do not contribute directly to the S2 binding pocket but may correctly position the two domains and consequently affect the specificity of the enzyme at this position.

S3 Subsite Specificity—There is little known about the S3 substrate specificity of OPB and the structure reveals only a single hydrogen bond from Ser-253 to the extended arm of the P3 guanidino group of AIP. However, the substrate specificity of the S3 subsite has been examined in both TcOPB and TbOPB, using kinetic analysis and it was found that the nature of the amino acid at P3 influenced the activity of both of these peptidases (47). In both enzymes, hydrophobic amino acids at position P3 produced among the best substrates. In OPB, the S3 binding pocket contains Leu-617 and Ser-253. Leu-617 is conserved in TcOPB and TbOPB and could easily

play a role in stabilizing a substrate through hydrophobic interactions at this position and hence contribute to the enzyme specificity in P3.

S1′ Subsite Specificity—In TcOPB and TbOPB the S1′ subsite was shown to be important in determining substrate specificity showing a preference for potential hydrogen-bond donors; Tyr, Ser, Thr and Gln at P1′(47). In OPB, a single phosphate moiety was found in the P1′ position stabilized by residues Try-496 and His-697, which are important in catalysis and Arg-576, which is conserved in the protozoa. This suggests that Arg-576 may be responsible for the preference of hydrogen-bond donors at this location. In addition, in the structure of mPEP (43), Val-458 and Gly-532 are suggested to play a role in substrate binding C-terminal of the scissile bond and Gly-532 overlays with Arg-576 in the crystal structures.

Substrate Route—The route of substrate entry into OPB is unknown but two different pathways and/or mechanisms have been proposed for entry into the catalytic domain of pPOP and mPEP (43, 52). However, neither one is directly applicable to OPB. In pPOP, a small tunnel at the inter-domain region, comprising a highly flexible N-terminal segment of the catalytic domain and a facing hydrophilic loop from the propeller domain (residues 192–205, Loop A (Fig. 3*a*)) was shown to be a potential pathway for the substrate (52). This loop is missing in both OPB and mPEP, suggesting that they have different substrate routes.

In mPEP, a salt bridge between Arg-572 (cat) and Asp-196/197 (prop), was proposed to function as a latch for the opening or closing of the two domains, to allow substrate entry into the active site (43). These residues are not structurally conserved in OPB (or pPOP) and there are no other salt bridges in the immediate vicinity. However, it is possible that another salt bridge (SB2; Glu-538 (cat) to Arg-302 (prop)) in OPB functions as a latch in a similar manner. As described above, Arg-302 adopts two conformations, one of which forms the salt bridge between the two domains. This is broken when it changes conformation and is replaced by an intra-domain salt bridge to Ser-271, when Arg-534 also changes its conformation. This type of switch may let the two domains of OPB to open and allow substrate entry as observed in mPEP (43). Overall, the domain interface of OPB is important for the both the functionality and substrate recognition properties of the enzyme.

Acknowledgments—We thank Gareth Westrop for providing the OPB expression plasmid, Mads Gabrielsen for discussion and extensive reading of the manuscript, and the European Synchrotron Radiation Facility for access.

REFERENCES

1. Barrett, A. J., and Rawlings, N. D. (1995) *Arch. Biochem. Biophys.* **318,** 247–250
2. Barrett, A. J., and Rawlings, N. D. (1992) *Biol. Chem. Hoppe Seyler* **373,** 353–360
3. Welches, W. R., Brosnihan, K. B., and Ferrario, C. M. (1993) *Life Sci.* **52,** 1461–1480
4. Rawlings, N. D., Morton, F. R., Kok, C. Y., Kong, J., and Barrett, A. J. (2008) *Nucleic Acids Res.* **36,** D320–D325
5. Venäläinen, J. I., Juvonen, R. O., and Männistö, P. T. (2004) *Eur. J. Biochem.* **271,** 2705–2715
6. Burleigh, B. A., and Woolsey, A. M. (2002) *Cell Microbiol.* **4,** 701–711
7. Coetzer, T. H., Goldring, J. P., and Huson, L. E. (2008) *Biochimie* **90,** 336–344
8. Burleigh, B. A., and Andrews, N. W. (1995) *Annu. Rev. Microbiol.* **49,** 175–200
9. Burleigh, B. A., Caler, E. V., Webster, P., and Andrews, N. W. (1997) *J. Cell Biol.* **136,** 609–620
10. Caler, E. V., Vaena de Avalos, S., Haynes, P. A., Andrews, N. W., and Burleigh, B. A. (1998) *EMBO J.* **17,** 4975–4986
11. Morty, R. E., Pellé, R., Vadász, I., Uzcanga, G. L., Seeger, W., and Bubis, J. (2005) *J. Biol. Chem.* **280,** 10925–10937
12. Troeberg, L., Pike, R. N., Morty, R. E., Berry, R. K., Coetzer, T. H., and Lonsdale-Eccles, J. D. (1996) *Eur J Biochem.* **238,** 728–736
13. Morty, R. E., Lonsdale-Eccles, J. D., Mentele, R., Auerswald, E. A., and Coetzer, T. H. (2001) *Infect. Immun.* **69,** 2757–2761
14. Morty, R. E., Troeberg, L., Powers, J. C., Ono, S., Lonsdale-Eccles, J. D., and Coetzer, T. H. (2000) *Biochem. Pharmacol.* **60,** 1497–1504
15. Ndung'u, J. M., Wright, N. G., Jennings, F. W., and Murray, M. (1992) *Parasitol. Res.* **78,** 553–556
16. Morty, R. E., Troeberg, L., Pike, R. N., Jones, R., Nickel, P., Lonsdale-Eccles, J. D., and Coetzer, T. H. (1998) *FEBS Lett.* **433,** 251–256
17. Ivens, A. C., Peacock, C. S., Worthey, E. A., Murphy, L., Aggarwal, G., Berriman, M., Sisk, E., Rajandream, M. A., Adlem, E., Aert, R., Anupama, A., Apostolou, Z., Attipoe, P., Bason, N., Bauser, C., Beck, A., Beverley, S. M., Bianchettin, G., Borzym, K., Bothe, G., Bruschi, C. V., Collins, M., Cadag, E., Ciarloni, L., Clayton, C., Coulson, R. M., Cronin, A., Cruz, A. K., Davies, R. M., De Gaudenzi, J., Dobson, D. E., Duesterhoeft, A., Fazelina, G., Fosker, N., Frasch, A. C., Fraser, A., Fuchs, M., Gabel, C., Goble, A., Goffeau, A., Harris, D., Hertz-Fowler, C., Hilbert, H., Horn, D., Huang, Y., Klages, S., Knights, A., Kube, M., Larke, N., Litvin, L., Lord, A., Louie, T., Marra, M., Masuy, D., Matthews, K., Michaeli, S., Mottram, J. C., Müller-Auer, S., Munden, H., Nelson, S., Norbertczak, H., Oliver, K., O'Neil, S., Pentony, M., Pohl, T. M., Price, C., Purnelle, B., Quail, M. A., Rabbinowitsch, E., Reinhardt, R., Rieger, M., Rinta, J., Robben, J., Robertson, L., Ruiz, J. C., Rutter, S., Saunders, D., Schäfer, M., Schein, J., Schwartz, D. C., Seeger, K., Seyler, A., Sharp, S., Shin, H., Sivam, D., Squares, R., Squares, S., Tosato, V., Vogt, C., Volckaert, G., Wambutt, R., Warren, T., Wedler, H., Woodward, J., Zhou, S., Zimmermann, W., Smith, D. F., Blackwell, J. M., Stuart, K. D., Barrell, B., and Myler, P. J. (2005) *Science* **309,** 436–442
18. Cheng, Y., and Prusoff, W. H. (1973) *Biochem. Pharmacol.* **22,** 3099–3108
19. Matthews, B. W. (1968) *J. Mol. Biol.* **33,** 491–497
20. Pflugrath, J. W. (1999) *Acta Crystallogr. D Biol. Crystallogr.* **55,** 1718–1725
21. Otwinowski, Z., and Minor, W. (1997) *Methods Enzymol.* **276,** 307–326
22. Collaborative Computational Project (1994) *Acta Crystallogr. D Biol. Crystallogr.* **50,** 760–763
23. delaFortelle, E., and Bricogne, G. (1997) *Methods Enzymol.* **276,** 472–494
24. Vonrhein, C., Blanc, E., Roversi, P., and Bricogne, G. (2007) *Methods Mol. Biol.* **364,** 215–230
25. Usón, I., and Sheldrick, G. M. (1999) *Curr. Opin. Struct. Biol.* **9,** 643–648
26. Abrahams, J. P., and Leslie, A. G. (1996) *Acta Crystallogr. D Biol. Crystallogr.* **52,** 30–42
27. Perrakis, A., Morris, R., and Lamzin, V. S. (1999) *Nat. Struct. Biol.* **6,** 458–463
28. Emsley, P., and Cowtan, K. (2004) *Acta Crystallogr. D* **60,** 2126–2132
29. McCoy, A. J. (2007) *Acta Crystallogr. D Biol. Crystallogr.* **63,** 32–41
30. Murshudov, G. N., Vagin, A. A., and Dodson, E. J. (1997) *Acta Crystallogr. D* **53,** 240–255
31. Davis, I. W., Murray, L. W., Richardson, J. S., and Richardson, D. C. (2004) *Nucleic Acids Res.* **32,** W615–W619
32. Velankar, S., Best, C., Beuth, B., Boutselakis, C. H., Cobley, N., Sousa Da Silva, A. W., Dimitropoulos, D., Golovin, A., Hirshberg, M., John, M., Krissinel, E. B., Newman, R., Oldfield, T., Pajon, A., Penkett, C. J.,

Pineda-Castillo, J., Sahni, G., Sen, S., Slowley, R., Suarez-Uruena, A., Swaminathan, J., van Ginkel, G., Vranken, W. F., Henrick, K., and Kleywegt, G. J. (2010) *Nucleic Acids Res.* **38,** D308–D317
33. Kanatani, A., Masuda, T., Shimoda, T., Misoka, F., Lin, X. S., Yoshimoto, T., and Tsuru, D. (1991) *J. Biochem.* **110,** 315–320
34. Kornblatt, M. J., Mpimbaza, G. W., and Lonsdale-Eccles, J. D. (1992) *Arch. Biochem. Biophys.* **293,** 25–31
35. Morty, R. E., Lonsdale-Eccles, J. D., Morehead, J., Caler, E. V., Mentele, R., Auerswald, E. A., Coetzer, T. H., Andrews, N. W., and Burleigh, B. A. (1999) *J. Biol. Chem.* **274,** 26149–26156
36. Morty, R. E., Authié, E., Troeberg, L., Lonsdale-Eccles, J. D., and Coetzer, T. H. (1999) *Mol. Biochem. Parasitol.* **102,** 145–155
37. Usuki, H., Uesugi, Y., Iwabuchi, M., and Hatanaka, T. (2009) *Biochim. Biophys. Acta* **1794,** 1673–1683
38. Ollis, D. L., Cheah, E., Cygler, M., Dijkstra, B., Frolow, F., Franken, S. M., Harel, M., Remington, S. J., Silman, I., and Schrag, J. (1992) *Protein Eng.* **5,** 197–211
39. Baker, S. C., Saunders, N. F., Willis, A. C., Ferguson, S. J., Hajdu, J., and Fülöp, V. (1997) *J. Mol. Biol.* **269,** 440–455
40. Neer, E. J., and Smith, T. F. (1996) *Cell* **84,** 175–178
41. Holm, L., Kääriäinen, S., Rosenström, P., and Schenkel, A. (2008) *Bioinformatics* **24,** 2780–2781
42. Fülöp, V., Böcskei, Z., and Polgár, L. (1998) *Cell* **94,** 161–170
43. Shan, L., Mathews, II, and Khosla, C. (2005) *Proc. Natl. Acad. Sci. U.S.A.* **102,** 3599–3604
44. Krissinel, E., and Henrick, K. (2004) *Acta Crystallogr. D* **60,** 2256–2268
45. Juhász, T., Szeltner, Z., Fülöp, V., and Polgár, L. (2005) *J. Mol. Biol.* **346,** 907–917
46. Schechter, I., and Berger, A. (1967) *Biochem. Biophys. Res. Commun.* **27,** 157–162
47. Hemerly, J. P., Oliveira, V., Del Nery, E., Morty, R. E., Andrews, N. W., Juliano, M. A., and Juliano, L. (2003) *Biochem. J.* **373,** 933–939
48. Morty, R. E., Fülöp, V., and Andrews, N. W. (2002) *J Bacteriol* **184,** 3329–3337
49. Lovell, S. C., Word, J. M., Richardson, J. S., and Richardson, D. C. (2000) *Proteins* **40,** 389–408
50. Krissinel, E., and Henrick, K. (2007) *J. Mol. Biol.* **372,** 774–797
51. Nicholls, A., Sharp, K. A., and Honig, B. (1991) *Proteins* **11,** 281–296
52. Fuxreiter, M., Magyar, C., Juhász, T., Szeltner, Z., Polgár, L., and Simon, I. (2005) *Proteins* **60,** 504–512
53. Heinig, M., and Frishman, D. (2004) *Nucleic Acids Res.* **32,** W500–502
54. Bond, C. S., and Schüttelkopf, A. W. (2009) *Acta Crystallogr. D Biol. Crystallogr.* **65,** 510–512
55. Bond, C. S. (2003) *Bioinformatics* **19,** 311–312
56. DeLano, W. L. (2002) *The PyMOL Molecular Graphics System*, San Carlos, CA